Title: Chloroplasts navigate towards the pathogen interface to counteract infection by the Irish potato famine pathogen

Authors: Alexia Toufexi[1†], Cian Duggan*[1†], Pooja Pandey[1], Zachary Savage[1], María Eugenia Segretin[3], Lok Him Yuen[1], David C. A. Gaboriau[2], Alexandre Y. Leary[1], Virendrasinh Khandare[1], Andrew D. Ward[4], Stanley W. Botchway[4], Benji C. Bateman[4], Indranil Pan[5,6], Martin Schattat[7], Imogen Sparkes[8], Tolga O. Bozkurt[1]*

Affiliations:

[1]Department of Life Sciences, Imperial College London, UK

[2]Facility for Imaging by Light Microscopy, NHLI, Faculty of Medicine, Imperial College London

[3]INGEBI-CONICET, Ciudad Autonoma de Buenos Aires, Argentina

[4]Central Laser Facility, Science and Technology Facilities Council Harwell, UK

[5]Centre for Process systems engineering and Centre for Environmental Policy, Imperial College London, UK

[6]The Alan Turing Institute, London, UK

[7]Martin-Luther-Universität Halle-Wittenberg, Germany

[8]School of Biological Sciences, University of Bristol, UK

*Correspondence to: o.bozkurt@imperial.ac.uk

[†]These authors contributed equally

Abstract: Chloroplasts are light harvesting organelles that arose from ancient endosymbiotic cyanobacteria. Upon immune activation, chloroplasts switch off photosynthesis, produce anti-microbial compounds, and develop tubular extensions called stromules. We report that chloroplasts navigate to the pathogen interface to counteract infection by the Irish potato famine pathogen *Phytophthora infestans*, physically associating with the specialised membrane that engulfs pathogen haustoria. Outer envelope protein, chloroplast unusual positioning1 (CHUP1), anchors chloroplasts to the host-pathogen interface. Stromules are induced during infection in a CHUP1-dependent manner, embracing haustoria and interconnecting chloroplasts, to form dynamic organelle clusters. Infection-triggered reprogramming of chloroplasts relies on surface immune signalling, whereas pathogen effectors subvert these immune pulses. Chloroplast are deployed focally, and coordinate to restrict pathogen entry into plant cells, a process actively countered by parasite effectors.

Introduction: *Phytophthora infestans* is an oomycete pathogen that causes potato late blight, one of the most historically and economically devastating crop diseases. The pathogen penetrates host cells via haustoria, infection structures that extend from its extracellular invasive hyphae. Haustoria are surrounded by the plant-derived extra-haustorial membrane (EHM), across which effectors secreted by the pathogen translocate inside the host cell (Wang et al., 2017; Whisson et al., 2016, 2007). This interface is key to the success or failure of infection and is therefore targeted by focal immune responses of the plant (Bozkurt et al., 2011; Dagdas et al., 2018; Kwon et al., 2008). Remarkably, despite being continuous with the plasma membrane, there is a stark difference in the biochemical composition of the EHM and the plasma membrane. EHM typically lacks surface localized pattern recognition receptors (PRRs), which activate downstream immune responses through recognition of pathogen associated molecular patterns (PAMPs) (Bozkurt et al., 2015, 2014). Activation of immunity at the cell surface stimulates chloroplasts to shut down photosynthesis, synthesize defence hormone precursors, and generate reactive oxygen species (ROS) (Padmanabhan and Dinesh-Kumar, 2010; Su et al., 2018), suggesting that chloroplasts are committed to the plant defence system. Additionally, chloroplasts produce stroma filled tubules (stromules) that have been implicated in defence (Caplan et al., 2015; Kumar et al., 2018). Pathogens are known to target chloroplasts with effector proteins (de Torres Zabala et al., 2015; Jelenska et al., 2007; Pecrix et al., 2018; Petre et al., 2016). Interestingly, several genes associated with resistance to oomycete pathogens were found to encode chloroplast-localized proteins (Belhaj et al., 2009; van Damme et al., 2009). However, the molecular and physiological mechanism of how chloroplast weaponry is launched against invading pathogens is unclear.

Here we show that to counteract host cell invasion by the Irish potato famine pathogen

P. infestans, chloroplasts navigate to pathogen penetration sites. Photo-relocation component chloroplast unusual positioning 1 (CHUP1) (Oikawa et al., 2008, 2003) mediates chloroplast accumulation around the haustorium by facilitating anchoring to the host-derived perimicrobial membrane interface. Moreover, stromule development increases upon *P. infestans* infection, in a CHUP1 dependent manner. Stromules embrace haustoria and mediate physical interactions between chloroplasts, forming dynamic clusters around the pathogen interface. Notably, infection-triggered stromule development relies on surface immune signalling, whereas the pathogen subverts this remotely by switching off surface immune pulses. These results implicate chloroplast photo-relocation machinery in plant focal immune responses and demonstrate that chloroplasts play a direct role in antagonizing pathogen invasion.

Results & Discussion:

To gain insights into defence-related chloroplast functions, we investigated chloroplast dynamics during *P. infestans* infection of the solanaceous model plant *Nicotiana benthamiana*. Confocal microscopy of infected leaf epidermal cells stably expressing GFP in chloroplast stroma (CpGFP hereafter) revealed that chloroplasts accumulate at 58% of haustoria (*n* = 299 haustoria) (Fig. 1A-C). Notably, chloroplasts are mainly positioned around infection sites, sieging haustoria in a highly dynamic fashion (Fig. 1C, 1E and Movie S1-3). Furthermore, compared to non-infected controls, we recorded a 5-fold increase in stromule formation in infected CpGFP cells (Fig. 1A-B, 1D). Notably, chloroplasts seized haustoria, tightly embracing the EHM through stromules that extend and coil around the pathogen (Fig. 1A, 1C, Movie S3). Expression of the EHM marker protein RFP:REM1.3 (Bozkurt et al., 2014) in infected CpGFP plants, allowed us to collect further evidence that chloroplasts intimately associate with the EHM (Fig. S1, Movie S4). Remarkably, time lapse-microscopy showed that chloroplasts plunge towards haustoria and embrace the EHM following haustorial penetration (Fig. 1E, Movie S5, Fig. S2), suggesting that chloroplasts may participate in focal immunity.

To determine the extent to which chloroplasts physically associate with the EHM, we next employed optical tweezers in combination with Total Internal Fluorescence Microscopy (TIRF) in infected CpGFP plants. Using optical tweezers, we successfully trapped and moved 17% of chloroplasts (*n* = 29) in non-haustoriated cells, a distance greater than the 10 µm threshold. In comparison, we were unable to trap and move any chloroplasts (0%, *n* = 18) neighbouring haustoria past the threshold, indicating a strong association between the chloroplasts and the EHM. Consistent with this, we recorded a few instances where these chloroplasts were initially pulled away from the EHM, but before they passed the distance threshold they escaped the trap and sprang back

95 towards their former position (22%, *n* = 18) (Fig. 1G, Movie S6). Taken together, these
96 results demonstrate that chloroplasts mobilize towards haustoria and tightly embrace the
97 EHM through induction of stromules, possibly to increase the surface area of interaction,
98 in a manner similar to chloroplast-nucleus communication upon activation of antiviral
99 immunity (Kumar et al., 2018).

100 Remarkably, upon pathogen infection, we noted that chloroplasts frequently formed
101 dynamic clusters via stromules, occasionally bridging multiple haustoria (Fig. 1A, Fig.
102 S3, Movie S1, S7, S8). Optical trapping of chloroplasts in pathogen-challenged tissue
103 illustrated co-migration of chloroplast pairs interconnected by a stromule like extension
104 (Fig. 1H, and Movie S9), indicating that chloroplasts can be physically linked. Both
105 observations raise the possibility that chloroplasts might coordinate their defence-related
106 tasks cooperatively to respond to pathogen attack. However whether plastids can fuse to
107 form a continuous stromal compartment that enables macromolecule exchange thorough
108 stromules is debated (Hanson and Hines, 2017; Schattat et al., 2014).

109 Intriguingly, although rarely observed, we captured two time-lapse image series, which
110 show collapse of the haustoria during chloroplast steering (Fig. S4, Movie S10, S11).
111 This prompted the idea that in addition to their biochemical arsenal (de Torres Zabala et
112 al., 2015; Serrano et al., 2016; Trotta et al., 2014), chloroplasts plausibly harness
113 mechanical means to oppose pathogen penetration. Supporting this view, we recorded
114 time-lapse series of chloroplast clusters adjacent to haustoria which moved
115 simultaneously in the same direction (Movie S12, S13).

116

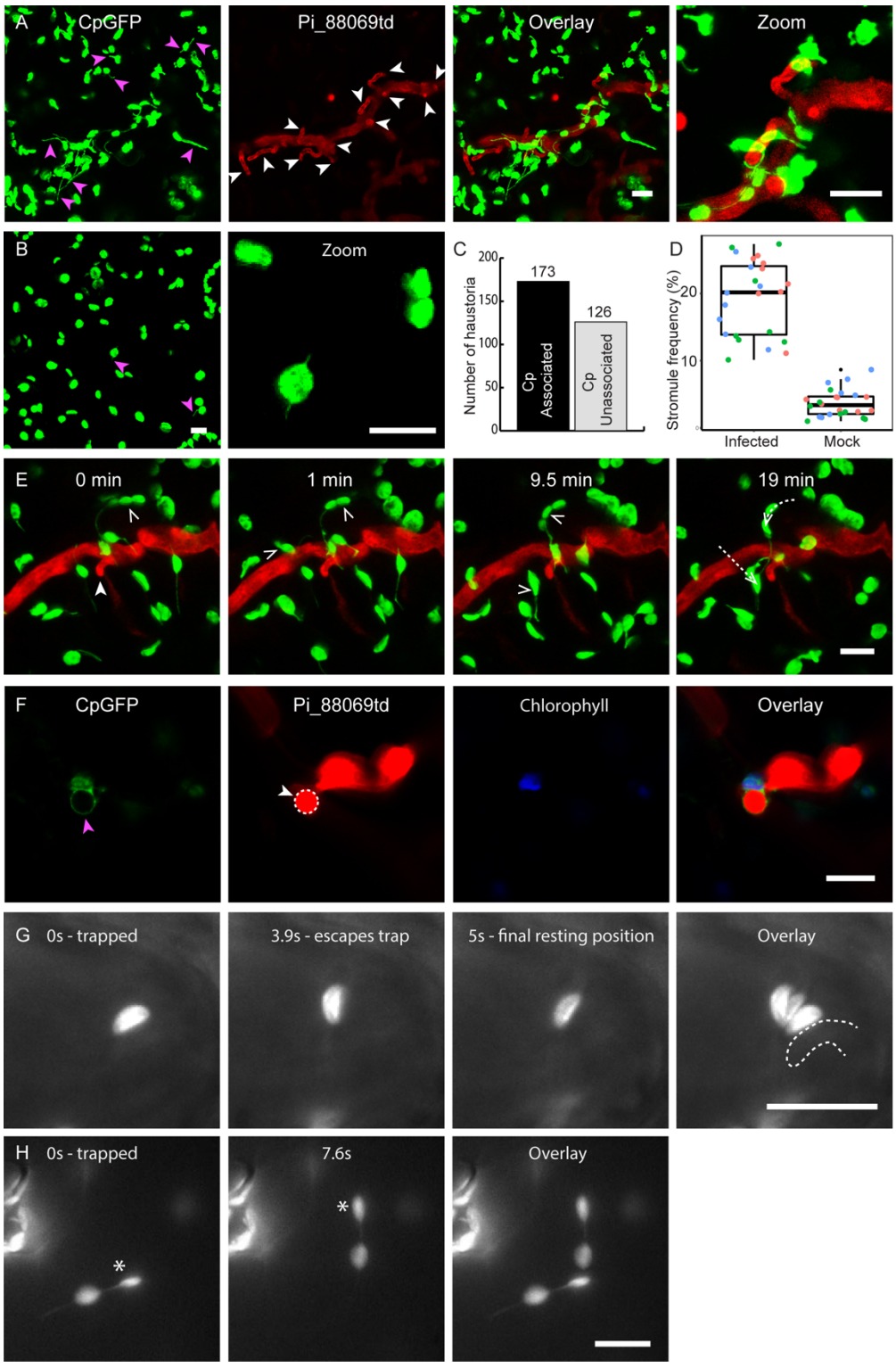

Fig. 1. Chloroplasts move towards haustoria and associate with the EHM via stromule induction. (A-B, E-F) Maximum projection confocal micrographs of *N. benthamiana* plants expressing GFP in chloroplast stroma (CpGFP). (A) Stromule

induction and chloroplast accumulation around haustoria with *P. infestans* strain 88069td compared to (B) Mock inoculated cells. (C) Number of 88069td haustoria associated with one or more chloroplast. (D) Scatter box-plot shows increased stromule induction ($p < 0.01$) in infected (n = 24 images quantified) vs uninfected (n = 24 images quantified) tissue. (E) Maximum intensity projection time-lapse series showing movement of tracked chloroplasts (open arrowheads) towards haustorium. Dashed line indicates approximate path travelled. (F) Single plane image showing stromule (purple arrowhead) wrapped around haustorium (white arrowhead). (G-H) GFP channel in grayscale from TIRF microscope. Time-lapse showing laser capture of haustorium associated chloroplast in CpGFP plant where automated the trapping routine, traps and attempts to move chloroplast 10 µm. (G) Chloroplast which escapes laser trap, reaching the furthest possible point from haustorium (3.9 s) before springing back (5.0 s). Dotted line shows outline of haustorium marked by RFP:REM1.3. (H) Trapped chloroplast (asterisk) linked by stromule to another chloroplast. When the trapped chloroplast moves, the linked chloroplast co-migrates. Scale bars: 10 µm.

To elucidate the role of chloroplast positioning in plant cell invasion of *P. infestans*, we investigated whether a relationship exists between light and pathogen-induced chloroplast movements. We particularly focused on chloroplast unusual positioning 1 (CHUP1), a protein that regulates chloroplast photo-relocation, movement and anchoring to the plasma membrane (Oikawa et al., 2008, 2003). Similar to a GFP fused chloroplast envelope marker protein, translocon at the outer membrane of chloroplasts 64 (TOC64:GFP), CHUP1:GFP labelled the chloroplast outer envelope (Fig 2A & B). However, CHUP1:GFP displayed an unusually increased fluorescence intensity at foci across the chloroplast-plasma membrane interface (Fig. 2A). Notably, in haustoriated cells, CHUP1:GFP accumulated at chloroplast-EHM contact sites (Fig. 2C, Fig. S5),

147 whereas TOC64:GFP uniformly labelled the chloroplast envelope without producing any
148 fluorescent foci adjacent to the EHM (Fig. 2D). The discrete punctate localisation of
149 CHUP1:GFP at the EHM contact sites suggested that CHUP1 could mediate anchoring
150 of chloroplasts to the EHM which typically lacks plasma membrane proteins (Bozkurt et
151 al., 2015, 2014; Whisson et al., 2016). These results indicate that CHUP1, a core
152 component of the chloroplast photo-relocation machinery, might be co-opted for
153 chloroplast recruitment to the pathogen interface.

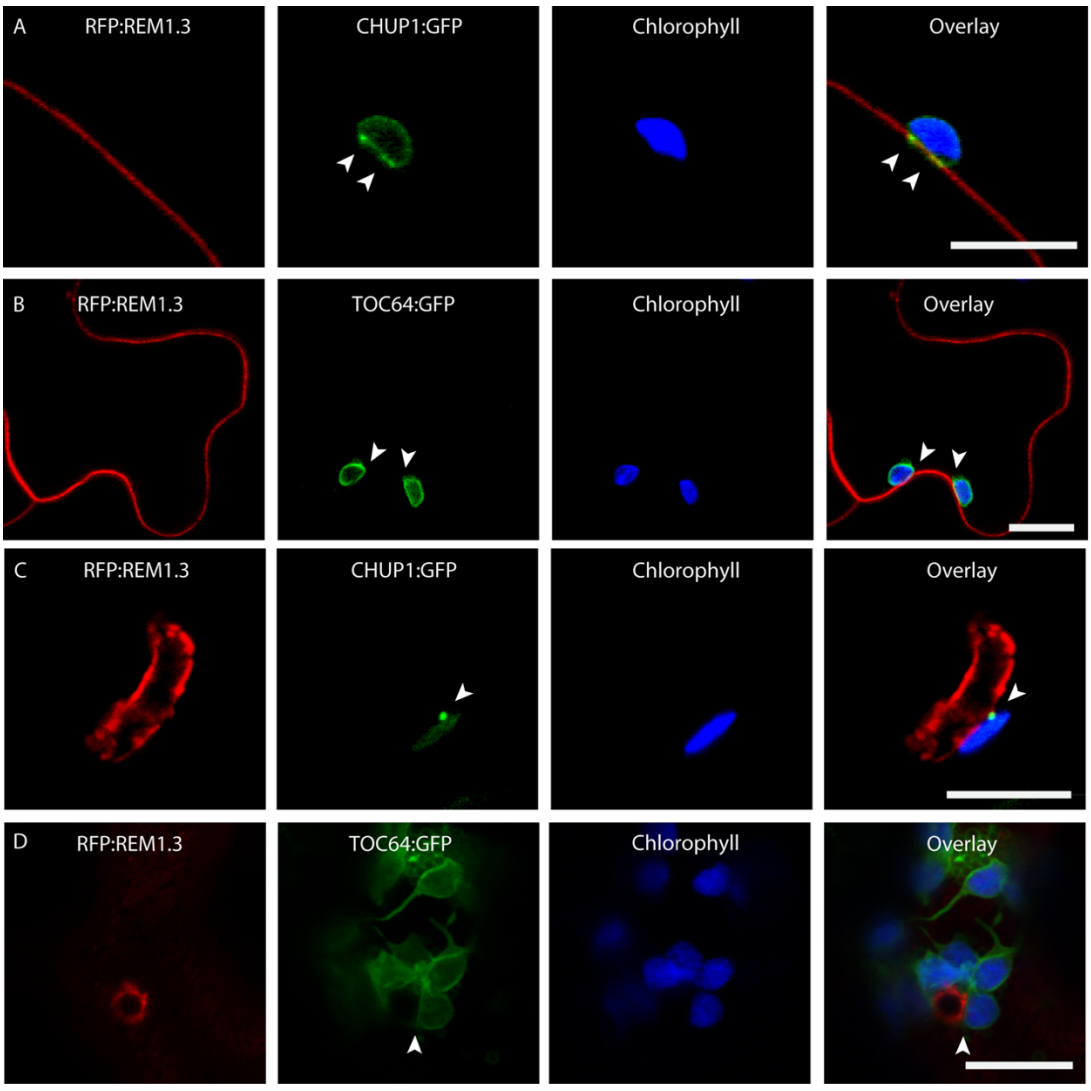

Fig. 2. CHUP1 localizes to the chloroplast outer envelope and accumulates at contact points between plastids and the plasma membrane or EHM. Single-plane confocal microscope images of wild-type *N. benthamiana* transiently co-expressing plasma membrane and EHM marker RFP:REM1.3 with CHUP1:GFP (A & C) or TOC64:GFP (B & D). (A) CHUP1:GFP labels chloroplast outer membrane and accumulates at contact points (white arrowheads) with the plasma membrane. (B) TOC64:GFP distributes uniformly across the chloroplast outer membrane. (C) CHUP1:GFP accumulates at *P. infestans* EHM contact points. (D) TOC64:GFP displays a uniform distribution when in contact with the EHM. Scale bars: 10 µm.

We next set out to determine whether CHUP1 is required for pathogen directed chloroplast movement and EHM docking. Remarkably, downregulation of *CHUP1* expression through virus-induced gene silencing (VIGS) in infected CpGFP plants, significantly reduced the number of haustoria that associate with chloroplasts (33%, *n* = 544 haustoria) compared to the silencing control (45%, *n* = 471 haustoria) (Fig. 3A-B, Fig. S6). We obtained similar results following RNA interference (RNAi) mediated knockdown of *CHUP1* in both wild-type *N. benthamiana* and CpGFP plants (Fig. S7). These results indicate that CHUP1 facilitates chloroplast recruitment to the pathogen interface, where it accumulates, likely through mediating chloroplast anchoring to the EHM (Fig. 2C). In addition, VIGS mediated knock down of *CHUP1* reduces stromule induction (8% chloroplasts with stromule(s), *n* = 68 images quantified) compared to control silencing (2% chloroplasts with stromule(s), *n* = 68 images quantified), suggesting that CHUP1 is required for pathogen induced stromule development (Fig. 3C). Likewise, in infected CpGFP plants, transient RNAi of CHUP1 led to a 2-fold decrease in stromule induction (18% chloroplasts with stromule(s), *n* = 11 images quantified) compared to the GUS-silencing control (39% chloroplasts with stromule(s), *n* = 10 images quantified) (Fig. S7). Collectively, these results demonstrate that CHUP1 is essential for both pathogen-directed chloroplast mobility and infection-triggered stromules formation which is implicated in antimicrobial immunity (Caplan et al., 2015), pointing to a positive role of CHUP1 in plant immunity.

We next tested the hypothesis that the process of chloroplast positioning and anchoring to the pathogen interface enhances disease resistance. VIGS of *CHUP1* led to considerably higher levels of *P. infestans* hyphal growth compared to the silencing control (Fig. 3D-E). We repeated these infection assays following RNAi-mediated silencing of *CHUP1*. Consistently, RNAi of *CHUP1* substantially enhanced filamentous

189 growth of *P. infestans* compared to RNAi-GUS control (Fig. 3F-G). Taken together,
190 these results indicate that CHUP1 contributes to plant focal immunity, possibly through
191 coordinating chloroplast navigation to the EHM. However, since CHUP1 is also essential
192 for induction of stromules that intimately associate with the EHM, we infer that processes
193 such as chloroplast steering and docking to the pathogen interface as well as formation
194 of stromules are a series of interconnected events to counteract microbial invasion.

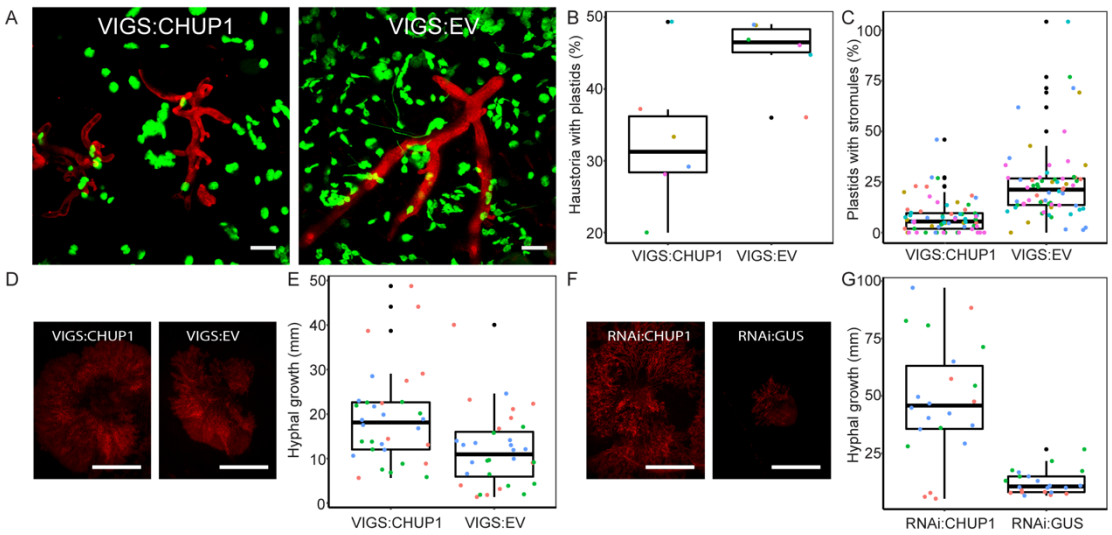

Fig. 3. CHUP1 silencing decreases immunity to *P. infestans*, perihaustorial chloroplast accumulation and stromule induction (A) Maximum-projection confocal micrographs of CpGFP leaf epidermal cells, where *CHUP1* is systemically silenced (VIGS), and infected with 88069td. VIGS-empty vector (EV) included as control. Scale bars: 10 µm. (B) Scatter-boxplot shows reduced percentage of haustoria associated with plastid(s) ($p < 0.01$) in VIGS-CHUP1 plants (33% of $n = 544$ haustoria), compared to VIGS-EV plants (45% of $n = 471$ haustoria). (C) Scatter-boxplot depicts reduction in stromule induction ($p < 0.01$) in VIGS-CHUP1 plants (8%, $n = 68$ images quantified), compared to VIGS-EV plants (24%, $n = 68$ images quantified). (D-G) Silencing of *CHUP1* by VIGS or transient RNAi, followed by 88069td inoculation shows CHUP1 contributes to resistance. Hyphal growth measured using fluorescence stereomicroscope at 4 dpi for VIGS (D) and 6 dpi for transient RNAi (F). Scale bars: 10 mm. (E & G) Scatter-boxplots show mean area of hyphal growth for inoculations on VIGS leaves, $n = 32$ leaves per treatment ($p < 0.01$) (E), and transient RNAi silenced leaves, $n = 22$ leaves for each experiment ($p < 0.01$).

Finally, to gain further insights into the interplay between chloroplasts and haustoria, we investigated the means of pathogen induced stromule formation. Stromule development was previously reported to be induced upon cytoplasmic recognition of bacterial effectors or viral particles by NLR (nucleotide-binding domain and leucine-rich repeat-containing) receptors (Caplan et al., 2015; Erickson et al., 2018; Krenz et al., 2012). However, because *P. infestans* establishes a compatible interaction with *N. benthamiana* without activating NLR triggered immunity, we reasoned that stromule development could be stimulated through surface immune recognition (Caplan et al., 2015). Thus, we monitored stromule formation upon silencing of *BAK1* (Fig. S8), a surface localized co-receptor that mediates immune signalling through various PRRs (Chaparro-Garcia et al., 2011; Perraki et al., 2018; Smakowska-Luzan et al., 2018). Remarkably, in five independent experiments, we noticed a substantial decrease in infection triggered stromule induction following *BAK1* silencing (4%, n = 37 images quantified) in relation to control silencing (23%, n = 37 images quantified) (Fig. 4A-B).

We then tested whether AVR3a, a host-translocated effector of *P. infestans* that suppresses BAK1-mediated immune signalling (Bos et al., 2010; Chaparro-Garcia et al., 2011), can perturb pathogen induced stromule development. Notably, following heterologous expression of AVR3a (Fig. S9), infection-triggered stromule formation decreased by more than two-fold (Fig. 4C-D). These results demonstrate that stromules are induced during *P. infestans* host colonization through surface immune signalling, whereas the pathogen deploys effectors to counteract this process, further supporting the defence-related role of stromules. Since stromule induction is CHUP1-dependent, we conclude that CHUP1 contributes to immunity through mediating chloroplast navigation and chloroplast interaction via diverse signalling stimuli, which are coordinated to prevent host cell invasion of filamentous pathogens (Fig. 4E, model).

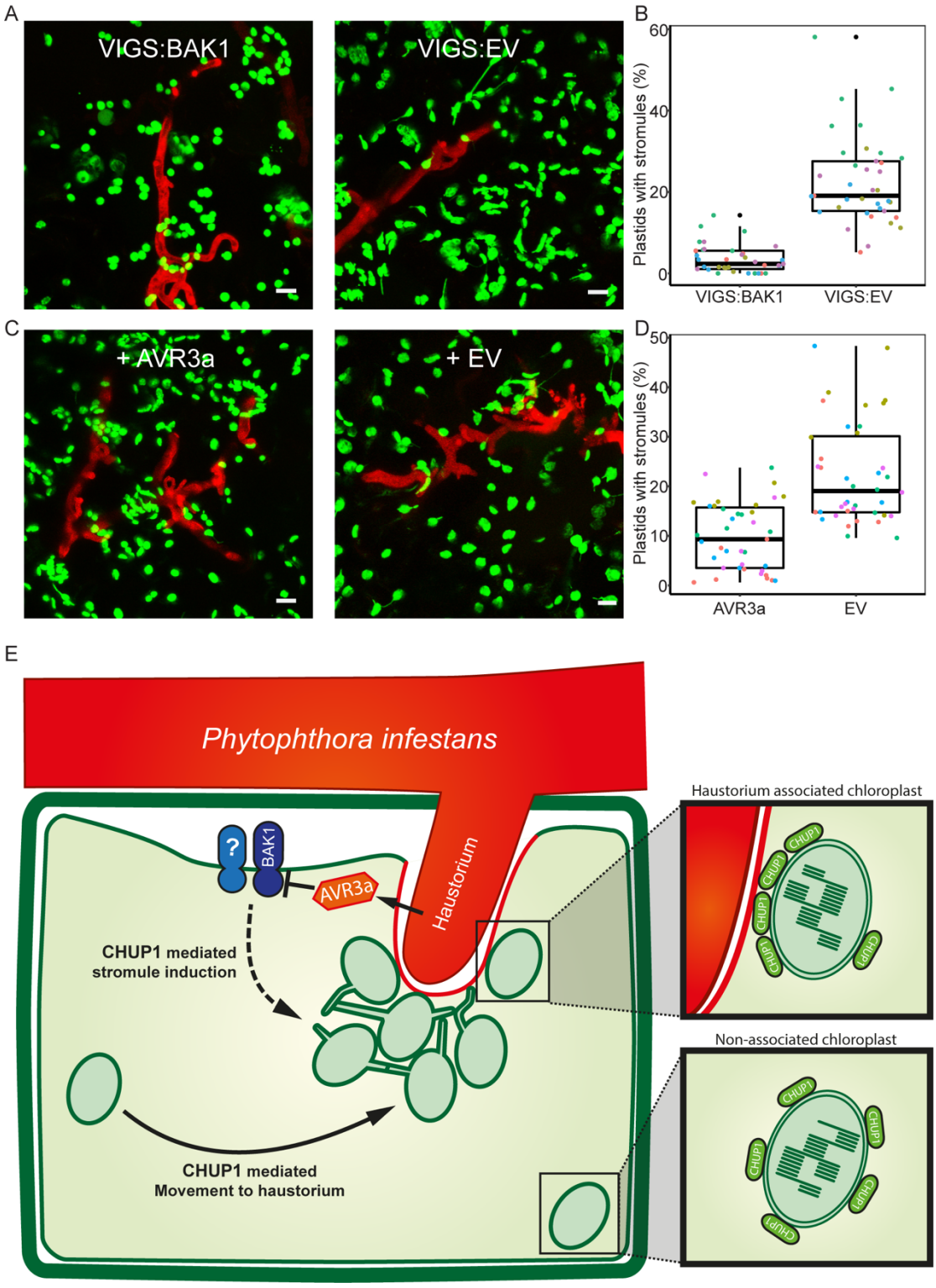

Fig. 4: *P. infestans* induces stromules through surface recognition. (A-B) Systemically silencing *BAK1* (VIGS-BAK1) reduces stromule induction during infection,

239 compared with EV control. (A) Maximum projection confocal microscopy images of
240 CpGFP leaves silenced with VIGS-BAK1 or VIGS-EV, infected with 88069td. (B) Scatter-
241 boxplot depicts reduction in stromule induction ($p < 0.01$) in VIGS-BAK1 plants (4%, n =
242 37 images quantified), compared to VIGS-EV plants (23%, n = 37 images quantified).
243 (C) Overexpression of *P. infestans* effector AVR3a reduces stromule induction during
244 infection with 88069td in CpGFP. (D) Scatter-boxplot shows transient AVR3a expression
245 reduces stromule induction (9%, n = 39 images quantified) compared to EV expression
246 (22%, n = 40 images quantified) ($p<0.01$). (E) Model: Surface recognition of *P. infestans*
247 leads to CHUP1-dependent stromule induction. CHUP1 mediates chloroplast movement
248 to siege haustoria and develop inter-chloroplast clustering at the penetration site.

Our results demonstrate that chloroplasts navigate to the pathogen interface and establish secure membrane contacts with the EHM to contribute to focal immunity (Fig. 1, Fig. S1-2, Movie S5). These processes are dependent on CHUP1, a key component of blue-light-induced chloroplast movement and plasma membrane attachment (Kasahara et al., 2002; Oikawa et al., 2008), indicating that chloroplast photo-relocation machinery is co-opted for antimicrobial immunity. Remarkably, CHUP1 accumulates at the chloroplast-EHM interface (Fig. 2C, Fig. S4), possibly to enable stronger membrane attachment, as has been shown in plasma membrane docking of chloroplasts (Kadota et al., 2009).

We show that surface immune activation induces stromule development into a large, intricate web of chloroplasts (Fig. 1A, 1H, Fig. S3, Movie S1, S3, S7-9). These are reminiscent of mitochondrial networks with poorly understood functions (Hoitzing et al., 2015). Intricate chloroplast clusters could boost coordination of their defence-related functions by, for instance, mediating focal deployment of chloroplast weaponry at the pathogen interface. In addition, a speculative hypothesis is that chloroplast clusters could also generate mechanical forces to repulse infection structures that invade the plant cells, as has been suggested by our live cell imaging (Fig. S10-13). However, we show that adapted pathogens can remotely counteract stromule development by deploying effectors that shut down surface immune signalling (Fig. 4B). Conceivably, this would dismantle chloroplast stromules and reduce the surface area of the chloroplasts in contact with the EHM. These findings further support the notion that stromules are induced to contribute to pathogen defence (Caplan et al., 2015; Erickson et al., 2018). Our findings implicate chloroplasts in polarized immune responses of plants against filamentous pathogens and point to more complex, direct defence-related functions for chloroplasts.

Materials and Methods

Biological Material

Nicotiana benthamiana plants grown in a growth chamber at 25°C under high light intensity (16-h-day/8-h-dark photoperiod) were used for all experiments. Transplastomic GFP-expressing *Nicotiana benthamiana* plants, accumulating GFP in the chloroplast stroma(Stegemann et al., 2012) were maintained in the same conditions. *Phytophthora infestans* isolate 88069 (WT)(Van West et al., 1998) and 88069td (TD)(Whisson et al., 2007), a transgenic strain expressing the red fluorescent marker tandem dimer RFP (tdTomato), were used. Both isolates were cultured on plates with rye sucrose agar (RSA) for 12-16 days at 18°C in the dark, as described elsewhere(Song et al., 2009) prior to use for infection of *N. benthamiana*.

Molecular Cloning and plasmid constructs

The following constructs used in this study were previously published as follows: RFP:REM1.3(Bozkurt et al., 2014); TOC64:GFP(Breuers et al., 2012); AVR3a cloned in pICSL86977 was provided by TSLSynBio. CHUP1:GFP construct was cloned using Gibson Assembly Protocol(Gibson et al., 2009). Briefly, CHUP1:GFP was generated by amplifying two PCR products (Phusion DNA polymerase, Thermo Scientific) from *N. benthamiana* cDNA, amplifying *CHUP1-a* (herein *CHUP1*) using two different primer pairs (CHUP1-A F; GA_CHUP1_R1; GA_CHUP1B_F2; GA_CHUP1B_R2). The PCR products were assembled and cloned into the destination vector pK7FWG2,0 (GFP) by Gibson assembly. The purified vector was transformed into *A. tumefaciens* competent cells. RNAi-silencing constructs for CHUP1 were cloned using the Gateway Cloning Technology. RNAi-CHUP1 construct was generated to target a region in the middle of

298 the gene (942-1200bp)(Helliwell and Waterhouse, 2003). The selected sequence was
299 synthetized and cloned into pK7GWIWG2(II) vector(Karimi et al., 2002). VIGS vector
300 pTRV2-CHUP1 was assembled by amplifying a 500bp region of *Chup1* (the same region
301 targeted as previously(Caplan et al., 2015)) from *N. benthamiana* cDNA using primers
302 VIGS-_CHUP1_F and VIGS_CHUP1_R2. The amplified fragment was then cloned into a
303 Gateway compatible pTRV2 vector using Gateway Technology (Invitrogen). Silencing
304 construct TRV2-BAK1 was kindly provided by The Sainsbury Lab(Chaparro-Garcia et
305 al., 2011).

306

307 Transient gene-expression assays in *N. benthamiana*

308 *Agrobacterium tumefaciens* GV3101 strain(Hellens et al., 2000) carrying T-DNA
309 constructs was used to mediate transient gene expression (Agroinfiltration) into 3-4-
310 week-old *N. benthamiana* leaves, as previously described(Bozkurt et al., 2014, 2011).
311 Briefly, overnight cultures of transformed *A. tumefaciens* were washed and harvested
312 with 1500 µl autoclaved dH_2O by centrifugation at 1500*g* twice and resuspended in
313 agroinfiltration buffer (10 mM 2-(*N*-morpholino-ethanesulfonic acid hydrate (MES
314 hydrate), 10 mM $MgCl_2$, pH 5.7). For the transient co-expression assays, each *A.*
315 *tumefaciens* construct was mixed in agroinfiltration buffer to achieve a final OD_{600} of 0.2
316 or 0.3 for each *A. tumefaciens*, depending on the experiment. *P. infestans* inoculations
317 were performed 4 to 24h after infiltrations.

318

319 Virus induced gene silencing (VIGS)

320 *Agrobacterium* was prepared as above carrying TRV1 and the appropriate TRV2
321 construct and mixed to a final OD_{600} of 0.4 or 0.2 respectively, in agroinfiltration buffer

322 supplemented with 100 µM acetosyringone (Sigma) and left in the dark for 2 h prior to
323 infiltration to stimulate virulence. 14-day old *N. benthamiana* seedlings were infiltrated in
324 both cotyledons and any true leaves that had emerged. *N. benthamiana* plants were
325 infiltrated with TRV1 and TRV2-CHUP1 for CHUP1-silencing and TRV1 and TRV2-EV
326 for the empty vector control. TRV2 containing the *N. benthamiana* sulfur (Su) gene
327 fragment (TRV2-NbSU) was used as a positive control to indicate viral spread. Plants
328 were left to grow under standard conditions until experiments could be carried out four
329 weeks later.

330

331 Infection assays

332 Infection assays to assess the effect of *CHUP1* silencing on *P. infestans* colonization
333 were performed as follow: for RNAi experiments, *A. tumefaciens* containing RNAi-
334 CHUP1 or RNAi-GUS (OD_{600} = 0.3) constructs were infiltrated for transient expression
335 side by side on either halves of independent *N. benthamiana* leaves, 24h prior to
336 infection. For VIGS experiments, 3 weeks after silencing was initiated leaves were
337 detached for infection from VIGS-CHUP1 and VIGS-empty vector plants. Zoospores
338 were harvested from sporangia by addition of cold distilled water and collected after 2h
339 of incubation at 4°C, adjusting dilution to 50,000 spores/ml. Infection assays were
340 performed by the addition of 10µl of zoospore droplets to the base, middle and tip of the
341 abaxial side of each leaf, 3 on each side, as described previously(Saunders et al., 2012;
342 Song et al., 2009). The infected leaves were maintained in plastic boxes on damp paper
343 towels at 18°C under 16-h- day/8-h-night conditions, and inoculated with *P. infestans*
344 88069td. Images of hyphal growth were captured on a Leica DFC300 FX fluorescent
345 microscope (Leica Microsystems, Germany) using the DSR UV filter at the timepoints
346 indicated in the Fig. legends. Images were processed in ImageJ (2.0) and quantification

of hyphal growth was performed by measuring the diameter in mm^2 of hyphal growth of each infected spot.

RT-PCR assay

60 mg of leaf tissue was excised from 4-week-old *N. benthamiana* leaves (RNAi experiment, 6 days after silencing), and 5-week old leaves (VIGS experiments) and frozen in liquid N_2. RNA was extracted from the leaf tissue using the Plant RNA Isolation Mini Kit Protocol (Agilent Technologies). RNA quality and concentration was measured using a NanoDropTM Lite Spectrophotometer (Thermo Scientific). cDNA was synthesized using as a template 2 µg of RNA following the SuperScript II RT protocol (Invitrogen). To amplify the cDNA, a standard PCR (RT-PCR) was then performed using DreamTaq DNA polymerase (5 u/µl) (Thermo Scientific). RNAi-CHUP1 construct effect on *CHUP1* downregulation was evaluated by RT-PCR using primers CHP1_RT_F1 and BD-CHUP1-REV. VIGS-CHUP1 silencing was confirmed with CHUP1a_RT_F & CHUP1a_RT_R, which specifically amplifies *CHUP1a*, and CHUP1b_RT_F & CHUP1b_RT_R, which specifically amplifies *CHUP1b.* VIGS-BAK1 silencing was confirmed as previously described(Chaparro-Garcia et al., 2011).

Confocal microscopy

All microscopy analyses were performed on live *N. benthamiana* epidermal cells 2-6 days post agroinfiltrations and infections. Leaf discs were excised and imaged on a Leica SP5 resonant inverted confocal microscope (Leica Microsystems) using 63X 1.2NA Plan-Apochromat water immersion objective. Specific excitation wavelengths and filters for emission spectra were set as described previously(Koh et al., 2005). The

Argon laser excitation was set to 488 nm and the Helium-Neon laser to 543 nm and their fluorescent emissions detected at 495–550 and 570–620 nm to visualize GFP and RFP fluorescence, respectively. To avoid bleed-through from different fluorophores, images were acquired using sequential scanning and Maximum Intensity Projections were created from the Z-stacks. 3D images and movies were generated with confocal files in 12-bit TIFF format imported into NIS-Elements (Version 4.50, Nikon Instruments, UK) and processed with Advanced Denoising. Movies were made using the Volume View and Movie Maker modules

Optical trapping setup

Optical trap for chloroplast/stromule capture was setup as described by Sparkes et al 2017, Chapter 13(Hawes, 2018, chap. 13). An optical trap with a two-channel TIRF microscope (TIRF-M) was combined with a Nikon Ti-U inverted microscope. Optical trapping was performed using a near infrared trapping laser at 1070 nm using a Nikon 100x, oil immersion, NA 1.49 TIRF objective lens. For GFP and RFP chromophores fused to the proteins of interest were excited using 488 and 561 nm laser diode, respectively. Their Fluorescent emissions were detected using two electron multiplying charge-coupled device (EMCCD, iXon, Andor) cameras. The sample (~5 mm^2 leaf tissue) was mounted on a computer-controlled variable speed (Märzhäuser) stepper motor stage. The associated computer-controlled hardware was interfaced using National Instruments LabVIEW which provides full automation for each trapping routine. The power of the optical trap laser transmission was set to 40.7 mW. The TIRF image was recorded from 0 s, the trap was turned on at 1 s, the translation stage movement of 10 µm at 2 µm/s begins at 5 s and ends at 10 s, the trap was deactivated at 11 s, and the image recording stops at 22 s (relating to 11 s recovery periods).

396 Bioinformatic and statistical analysis

397 In order to identify putative orthologs of *Arabidopsis thaliana* for CHUP1 in *N.*
398 *benthamiana* genome, a TBLASTN search using the protein sequence of *CHUP1* from
399 *A. thaliana* against the *N. benthamiana* cDNA was accomplished in Solgenomics. Two
400 orthologs (*CHUP1-a* and *CHUP1-b*) of *Arabidopsis CHUP1* gene were identified in *N.*
401 *benthamiana* genome. Chloroplast quantification was done automatically using a
402 MATLAB script. Stromules were manually counted using a semi-automated MATLAB
403 script. Percentage of chloroplasts with stromules were calculated by dividing the number
404 of chloroplasts one (or more) stromule(s) by the total number of chloroplasts.
405 Quantification of hyphal growth was accomplished by measuring the diameter of the
406 lesion on each inoculated spot using Fiji image-processing software. R package was
407 used to visualize the values from three to four independent biological replicates by
408 generating scatter plots. Statistical significance of the differences observed were
409 assessed by t test when found to be normal by sharpiro test. If data was found to be
410 non-normally distributed Wilcox statistical test was implemented by R package.

411

412 Chloroplast automated counting algorithm through image processing

413 The image processing algorithms were used to calculate the gradient of the image to
414 identify the boundaries of the puncta. Enclosed regions formed by the boundaries were
415 algorithmically identified and counted. This procedure was done for each individual
416 channel green (in chloroplast stroma) and blue (Chloroplast Auto-fluorescence). The
417 chloroplast (GFP channel) containing stromule were counted in a semi-automated
418 fashion.

Acknowledgements: We thank Dr. Alex Jones (Warwick) for initiating collaboration with IS, Dr. Sebastian Schornack (SLCU) for initiating collaboration with MS, Prof. Peter Nixon (Imperial) for providing CP-GFP plant seeds. **Funding:** Bozkurt lab funded by BBSRC (BB/M002462/1). The Facility for Imaging by Light Microscopy (FILM) at Imperial College London is part-supported by funding from the Wellcome Trust (grant 104931/Z/14/Z) and BBSRC (grant BB/L015129/1). **Author contributions:** Conceptualization: CD, ZS, MES, IS, MS, TOB; Data curation: AT, CD, PP, ZS, DCAG, BCB, LHY, IS, TOB; Formal analysis: AT, CD, PP, ZS, BCB, IS, TOB; Funding acquisition: TOB; Investigation: AT, CD, PP, ZS, MES, LHY, AYL, VK, BCB, TOB; Methodology: AT, CD, ZS, DCAG, ADW, SWB, BCB, IS, MS, TOB; Project Administration: CD, TOB; Resources: AT, CD, AYL, VK, IP, IS, TOB; Software: IP; Supervision: AT, CD, PP, MES, BCB, IS, TOB; Validation: AT, CD, PP, ZS, MES, IS, MS; Visualisation: CD, ZS, TOB; Writing – original draft: CD, ZS, TOB; Writing – review & editing: AT, CD, PP, ZS, MES, LHY, DCAG, AYL, ADW, SWB, MS, IS, TOB. **Competing interests:** Authors declare no competing interests. **Data and materials availability:** All data is available in the main text, the supplementary materials or other raw data is available upon request. We are happy to provide all materials used here upon request.

437 **References:**

438 Belhaj K, Lin B, Mauch F. 2009. The chloroplast protein RPH1 plays a role in the
439 immune response of Arabidopsis to Phytophthora brassicae. *Plant J* **58**:287–298.
440 doi:10.1111/j.1365-313X.2008.03779.x

441 Bos JIB, Armstrong MR, Gilroy EM, Boevink PC, Hein I, Taylor RM, Zhendong T,
442 Engelhardt S, Vetukuri RR, Harrower B, Dixelius C, Bryan G, Sadanandom A,
443 Whisson SC, Kamoun S, Birch PRJ. 2010. Phytophthora infestans effector AVR3a
444 is essential for virulence and manipulates plant immunity by stabilizing host E3
445 ligase CMPG1. *Proc Natl Acad Sci* **107**:9909–9914. doi:10.1073/pnas.0914408107

446 Bozkurt TO, Belhaj K, Dagdas YF, Chaparro-Garcia A, Wu C-H, Cano LM, Kamoun S.
447 2015. Rerouting of plant late endocytic trafficking toward a pathogen interface.
448 *Traffic* **16**:204–26. doi:10.1111/tra.12245

449 Bozkurt TO, Richardson A, Dagdas YF, Mongrand S, Kamoun S, Raffaele S. 2014. The
450 Plant Membrane-Associated REMORIN1.3 Accumulates in Discrete Perihaustorial
451 Domains and Enhances Susceptibility to Phytophthora infestans. *Plant Physiol*
452 **165**:1005–1018. doi:10.1104/pp.114.235804

453 Bozkurt TO, Schornack S, Win J, Shindo T, Ilyas M, Oliva R, Cano LM, Jones AME,
454 Huitema E, van der Hoorn R a L, Kamoun S. 2011. Phytophthora infestans effector
455 AVRblb2 prevents secretion of a plant immune protease at the haustorial interface.
456 *Proc Natl Acad Sci U S A* **108**:20832–7. doi:10.1073/pnas.1112708109

457 Breuers FKH, Bräutigam A, Geimer S, Welzel UY, Stefano G, Renna L, Brandizzi F,
458 Weber APM. 2012. Dynamic Remodeling of the Plastid Envelope Membranes – A
459 Tool for Chloroplast Envelope in vivo Localizations. *Front Plant Sci* **3**:1–10.
460 doi:10.3389/fpls.2012.00007

461 Brodersen P, Achard, Lali Sakvarelidze Rasmussen MB, Dunoyer P, Yamamoto YY,
462 Sieburth L, Voinnet O. 2008. Widespread Translational Inhibition by Plant miRNAs

463 and siRNAs. *Science (80-)* **320**:1185–1190.

464 Caplan JL, Kumar AS, Park E, Padmanabhan MS, Hoban K, Modla S, Czymmek K,
465 Dinesh-Kumar SP. 2015. Chloroplast Stromules Function during Innate Immunity.
466 *Dev Cell* **34**:45–57. doi:10.1016/j.devcel.2015.05.011

467 Chaparro-Garcia A, Wilkinson RC, Gimenez-Ibanez S, Findlay K, Coffey MD, Zipfel C,
468 Rathjen JP, Kamoun S, Schornack S. 2011. The receptor-like kinase serk3/bak1 is
469 required for basal resistance against the late blight pathogen Phytophthora
470 infestans in Nicotiana benthamiana. *PLoS One* **6**.
471 doi:10.1371/journal.pone.0016608

472 Dagdas YF, Pandey P, Tumtas Y, Sanguankiattichai N, Belhaj K, Duggan C, Leary AY,
473 Segretin ME, Contreras MP, Savage Z, Khandare VS, Kamoun S, Bozkurt TO.
474 2018. Host autophagy machinery is diverted to the pathogen interface to mediate
475 focal defense responses against the Irish potato famine pathogen. *Elife* 1–15.
476 doi:10.7554/eLife.37476

477 de Torres Zabala M, Littlejohn G, Jayaraman S, Studholme D, Bailey T, Lawson T,
478 Tillich M, Licht D, Bölter B, Delfino L, Truman W, Mansfield J, Smirnoff N, Grant M.
479 2015. Chloroplasts play a central role in plant defence and are targeted by
480 pathogen effectors. *Nat Plants* **1**:15074. doi:10.1038/nplants.2015.74

481 Erickson JL, Adlung N, Lampe C, Bonas U, Schattat MH. 2018. The Xanthomonas
482 effector XopL uncovers the role of microtubules in stromule extension and
483 dynamics in Nicotiana benthamiana. *Plant J* **93**:856–870. doi:10.1111/tpj.13813

484 Gibson DG, Young L, Chuang R-Y, Venter JC, Hutchison CA, Smith HO. 2009.
485 Enzymatic assembly of DNA molecules up to several hundred kilobases. *Nat*
486 *Methods* **6**:343–5. doi:10.1038/nmeth.1318

487 Hanson MR, Hines KM. 2017. Stromules: Probing Formation and Function. *Plant Physiol*
488 **176**:pp.01287.2017. doi:10.1104/pp.17.01287

489 Hawes C. 2018. The Plant Endoplasmic Reticulum, Methods in Molecular Biology. New
490 York, NY: Springer New York. doi:10.1007/978-1-4939-7389-7
491 Hellens R, Mullineaux P, Klee H. 2000. Technical Focus:a guide to Agrobacterium binary
492 Ti vectors. *Trends Plant Sci* **5**:446–51.
493 Helliwell C, Waterhouse P. 2003. Constructs and methods for high-throughput gene
494 silencing in plants. *Methods* **30**:289–95.
495 Hoitzing H, Johnston IG, Jones NS. 2015. What is the function of mitochondrial
496 networks? A theoretical assessment of hypotheses and proposal for future
497 research. *BioEssays* **37**:687–700. doi:10.1002/bies.201400188
498 Jelenska J, Yao N, Vinatzer BA, Wright CM, Brodsky JL, Greenberg JT. 2007. A J
499 Domain Virulence Effector of Pseudomonas syringae Remodels Host Chloroplasts
500 and Suppresses Defenses. *Curr Biol* **17**:499–508. doi:10.1016/j.cub.2007.02.028
501 Kadota A, Yamada N, Suetsugu N, Hirose M, Saito C, Shoda K, Ichikawa S, Kagawa T,
502 Nakano A, Wada M. 2009. Short actin-based mechanism for light-directed
503 chloroplast movement in Arabidopsis. *Proc Natl Acad Sci* **106**:13106–13111.
504 doi:10.1073/pnas.0906250106
505 Karimi M, Inzé D, Depicker A. 2002. GATEWAY vectors for Agrobacterium-mediated
506 plant transformation. *Trends Plant Sci* **7**:193–5. doi:10.1016/S1360-1385(02)02251-
507 3
508 Kasahara M, Kagawa T, Oikawa K, Suetsugu N, Miyao M, Wada M. 2002. Chloroplast
509 avoidance movement reduces photodamage in plants. *Nature* **420**:829–832.
510 doi:10.1038/nature01213
511 Koh S, André A, Edwards H, Ehrhardt D, Somerville S. 2005. Arabidopsis thaliana
512 subcellular responses to compatible Erysiphe cichoracearum infections. *Plant J*
513 **44**:516–529. doi:10.1111/j.1365-313X.2005.02545.x
514 Krenz B, Jeske H, Kleinow T. 2012. The induction of stromule formation by a plant DNA-

515 virus in epidermal leaf tissues suggests a novel intra- and intercellular
516 macromolecular trafficking route. *Front Plant Sci* **3**:1–12.
517 doi:10.3389/fpls.2012.00291
518 Kumar AS, Park E, Nedo A, Alqarni A, Ren L, Hoban K, Modla S, McDonald JH,
519 Kambhamettu C, Dinesh-Kumar SP, Caplan JL. 2018. Stromule extension along
520 microtubules coordinated with actin-mediated anchoring guides perinuclear
521 chloroplast movement during innate immunity. *Elife* **7**:1–33.
522 doi:10.7554/eLife.23625
523 Kwon C, Neu C, Pajonk S, Yun HS, Lipka U, Humphry M, Bau S, Straus M, Kwaaitaal M,
524 Rampelt H, El Kasmi F, Jürgens G, Parker J, Panstruga R, Lipka V, Schulze-Lefert
525 P. 2008. Co-option of a default secretory pathway for plant immune responses.
526 *Nature* **451**:835–40. doi:10.1038/nature06545
527 Oikawa K, Kasahara M, Kiyosue T, Kagawa T, Suetsugu N, Takahashi F, Kanegae T,
528 Niwa Y, Kadota A, Wada M. 2003. Chloroplast unusual positioning1 is essential for
529 proper chloroplast positioning. *Plant Cell* **15**:2805–15. doi:10.1105/tpc.016428
530 Oikawa K, Yamasato A, Kong S-G, Kasahara M, Nakai M, Takahashi F, Ogura Y,
531 Kagawa T, Wada M. 2008. Chloroplast Outer Envelope Protein CHUP1 Is Essential
532 for Chloroplast Anchorage to the Plasma Membrane and Chloroplast Movement.
533 *Plant Physiol* **148**:829–842. doi:10.1104/pp.108.123075
534 Padmanabhan MS, Dinesh-Kumar SP. 2010. All Hands on Deck—The Role of
535 Chloroplasts, Endoplasmic Reticulum, and the Nucleus in Driving Plant Innate
536 Immunity. *Mol Plant-Microbe Interact* **23**:1368–1380. doi:10.1094/MPMI-05-10-0113
537 Pecrix Y, Buendia L, Penouilh-Suzette C, Maréchaux M, Legrand L, Bouchez O, Rengel
538 D, Gouzy J, Cottret L, Vear F, Godiard L. 2018. Sunflower resistance to multiple
539 downy mildew pathotypes revealed by recognition of conserved effectors of the
540 oomycete *Plasmopara halstedii*. *Plant J*. doi:10.1111/tpj.14157

541 Perraki A, DeFalco TA, Derbyshire P, Avila J, Séré D, Sklenar J, Qi X, Stransfeld L,
542 Schwessinger B, Kadota Y, Macho AP, Jiang S, Couto D, Torii KU, Menke FLH,
543 Zipfel C. 2018. Phosphocode-dependent functional dichotomy of a common co-
544 receptor in plant signalling. *Nature* **561**:248–252. doi:10.1038/s41586-018-0471-x
545 Petre B, Lorrain C, Saunders DGO, Win J, Sklenar J, Duplessis S, Kamoun S. 2016.
546 Rust fungal effectors mimic host transit peptides to translocate into chloroplasts.
547 *Cell Microbiol* **18**:453–465. doi:10.1111/cmi.12530
548 Saunders DGO, Breen S, Win J, Schornack S, Hein I, Bozkurt TO, Champouret N,
549 Vleeshouwers VG a a, Birch PRJ, Gilroy EM, Kamoun S. 2012. Host protein BSL1
550 associates with Phytophthora infestans RXLR effector AVR2 and the Solanum
551 demissum Immune receptor R2 to mediate disease resistance. *Plant Cell* **24**:3420–
552 34. doi:10.1105/tpc.112.099861
553 Schattat MH, Barton KA, Mathur J. 2014. The myth of interconnected plastids and
554 related phenomena. *Protoplasma* **252**:359–371. doi:10.1007/s00709-014-0666-4
555 Serrano I, Audran C, Rivas S. 2016. Chloroplasts at work during plant innate immunity. *J*
556 *Exp Bot* **67**:3845–3854. doi:10.1093/jxb/erw088
557 Smakowska-Luzan E, Mott GA, Parys K, Stegmann M, Howton TC, Layeghifard M,
558 Neuhold J, Lehner A, Kong J, Grünwald K, Weinberger N, Satbhai SB, Mayer D,
559 Busch W, Madalinski M, Stolt-Bergner P, Provart NJ, Mukhtar MS, Zipfel C,
560 Desveaux D, Guttman DS, Belkhadir Y. 2018. An extracellular network of
561 Arabidopsis leucine-rich repeat receptor kinases. *Nature* **553**:342–346.
562 doi:10.1038/nature25184
563 Song J, Win J, Tian M, Schornack S, Kaschani F, Ilyas M, Hoorn RAL Van Der, Kamoun
564 S. 2009. Apoplastic effectors secreted by two unrelated eukaryotic plant pathogens
565 target the tomato defense protease Rcr3.
566 Stegemann S, Keuthe M, Greiner S, Bock R. 2012. Horizontal transfer of chloroplast

genomes between plant species. *Proc Natl Acad Sci* **109**:2434–2438. doi:10.1073/pnas.1114076109

Su J, Yang L, Zhu Q, Wu H, He Y, Liu Y, Xu J, Jiang D, Zhang S. 2018. Active photosynthetic inhibition mediated by MPK3/MPK6 is critical to effector-triggered immunity. *PLoS Biol* **16**:1–29. doi:10.1371/journal.pbio.2004122

Trotta A, Rahikainen M, Konert G, Finazzi G, Kangasjärvi S. 2014. Signalling crosstalk in light stress and immune reactions in plants. *Philos Trans R Soc Lond B Biol Sci* **369**:20130235. doi:10.1098/rstb.2013.0235

van Damme M, Zeilmaker T, Elberse J, Andel A, de Sain-van der Velden M, van den Ackerveken G. 2009. Downy Mildew Resistance in Arabidopsis by Mutation of HOMOSERINE KINASE. *Plant Cell Online* **21**:2179–2189. doi:10.1105/tpc.109.066811

Van West P, De Jong AJ, Judelson HS, Emons AMC, Govers F. 1998. The ipiO gene of phytophthora infestans is highly expressed in invading hyphae during infection. *Fungal Genet Biol* **23**:126–138. doi:10.1006/fgbi.1998.1036

Wang S, Boevink PC, Welsh L, Zhang R, Whisson SC, Birch PRJ. 2017. Delivery of cytoplasmic and apoplastic effectors from *Phytophthora infestans* haustoria by distinct secretion pathways. *New Phytol*. doi:10.1111/nph.14696

Whisson SC, Boevink PC, Moleleki L, Avrova AO, Morales JG, Gilroy EM, Armstrong MR, Grouffaud S, Van West P, Chapman S, Hein I, Toth IK, Pritchard L, Birch PRJ. 2007. A translocation signal for delivery of oomycete effector proteins into host plant cells. *Nature* **450**:115–118. doi:10.1038/nature06203

Whisson SC, Boevink PC, Wang S, Birch PR. 2016. The cell biology of late blight disease. *Curr Opin Microbiol* **34**:127–135. doi:10.1016/j.mib.2016.09.002

List of Supplementary Materials:

Figures S1-S9

Table S1

Movies S1-S13

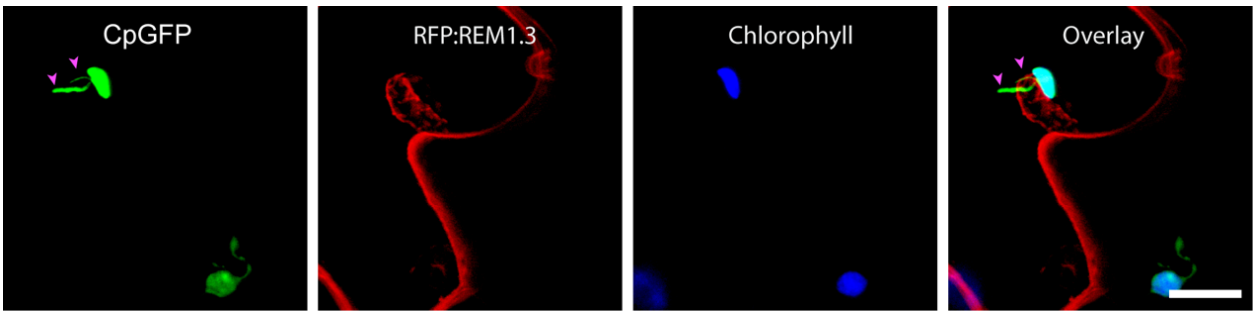

Fig. S1: Confocal micrographs showing a chloroplast embracing a haustorium with its stromules. Leaf epidermal cells from transplastomic CpGFP *N. benthamiana* plants transiently expressing plasma membrane and EHM marker RFP:REM1.3 were infected with WT *P. infestans* 8806 and imaged 4dpi. Blue represents chlorophyll autofluorescence. Scale bar is 10 µm. Magenta arrowheads indicate stromules.

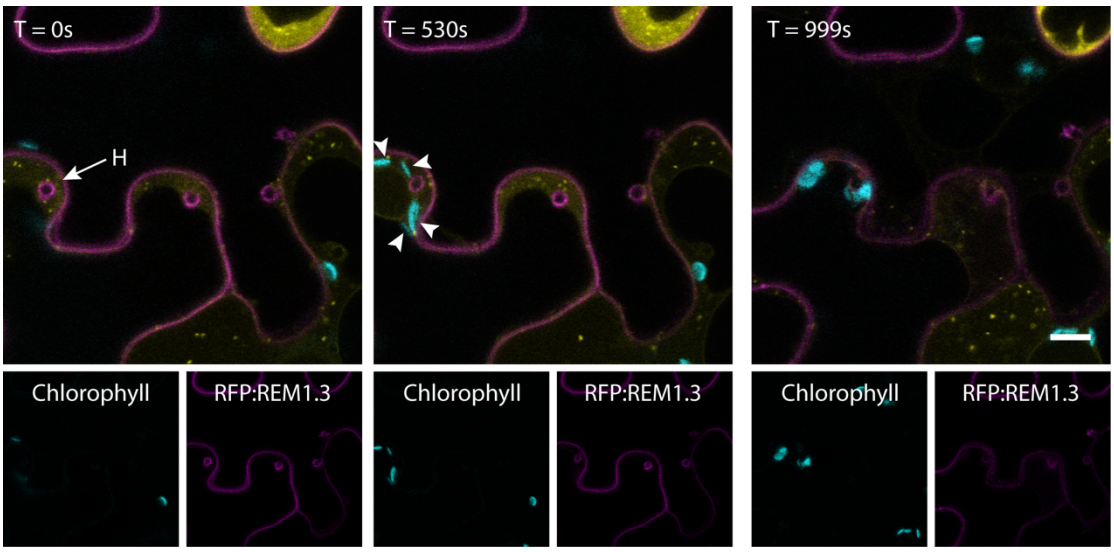

Fig. S2: Time-lapse series showing chloroplasts accumulation towards a haustorium. Leaf epidermal cells from WT *N. benthamiana* plants expressing PM and EHM marker RFP:REM1.3 (Magenta) and endosomal marker GFP:RAB8 (Yellow) infected with WT *P. infestans* 88069. Cyan is chlorophyll autofluorescence, labelling the chloroplasts. Scale bar is 10 µm.

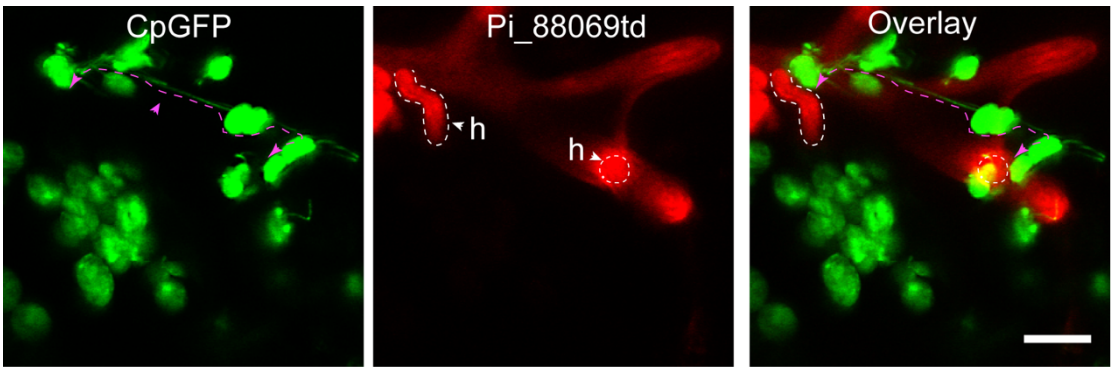

Fig. S3: Chloroplasts form long-distance stromule interactions that can bridge more than one haustorium. Confocal micrographs of leaf epidermal cells from transplastomic CpGFP *N. benthamiana* plants. Maximum intensity projection (10 images), 5 dpi (days post infection) with red-fluorescent *P. infestans* strain 88069td. 'h' indicates haustorium, Magenta arrowheads indicate long-distance stromule interactions. Scale bars are 10 µm. See 3D Movie 7.

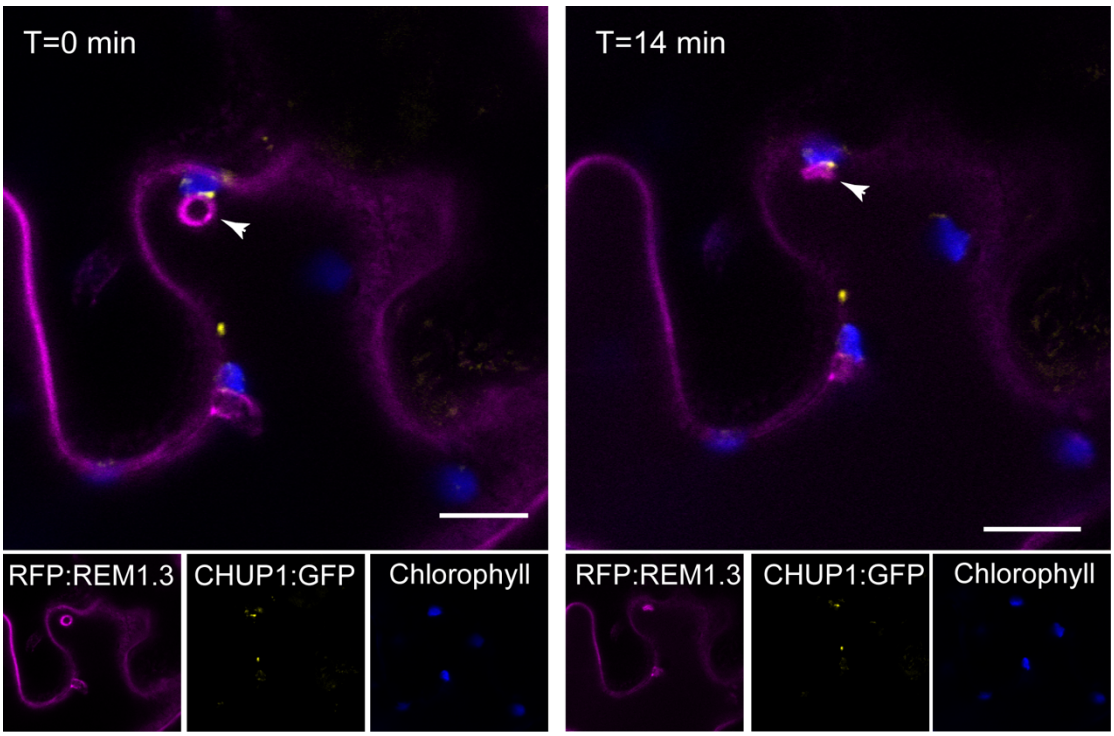

Fig. S4: Time-lapse series showing collapse of haustorium. *N. benthamiana* leaves transiently co-expressing plasma membrane and EHM marker RFP:REM1.3 with CHUP1:GFP. Arrowhead indicates haustorium that collapses. Scale bars are 10 µm.

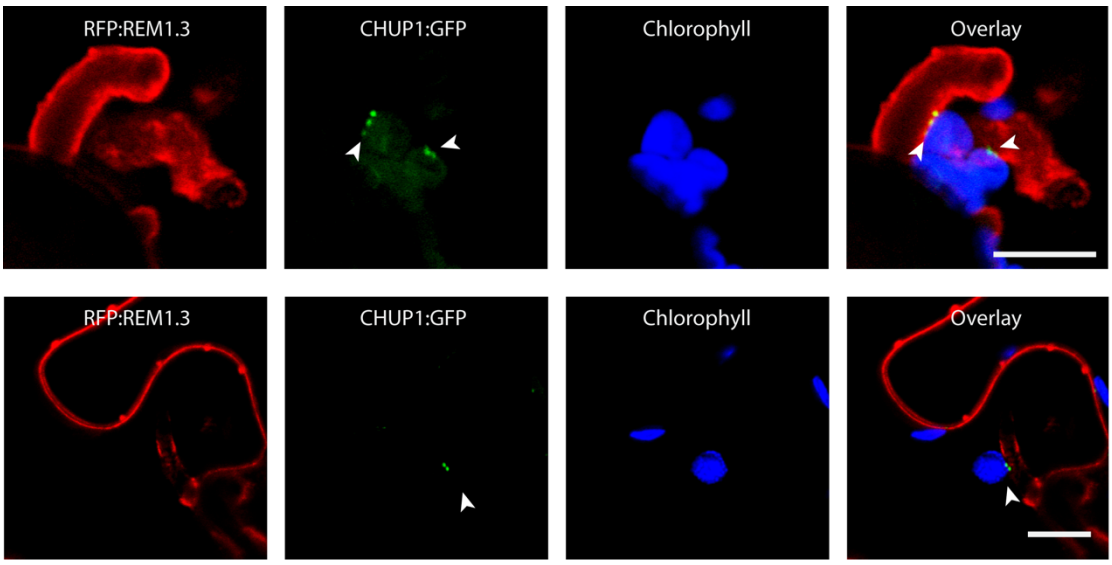

Fig. S5: CHUP1:GFP accumulates at the contact points between the chloroplast and the EHM. *N. benthamiana* leaves transiently co-expressing plasma membrane and EHM marker RFP:REM1.3 with CHUP1:GFP were infected with WT *P. infestans* 88069. Blue represents chlorophyll autofluorescence. Scale bars are 10 µm.

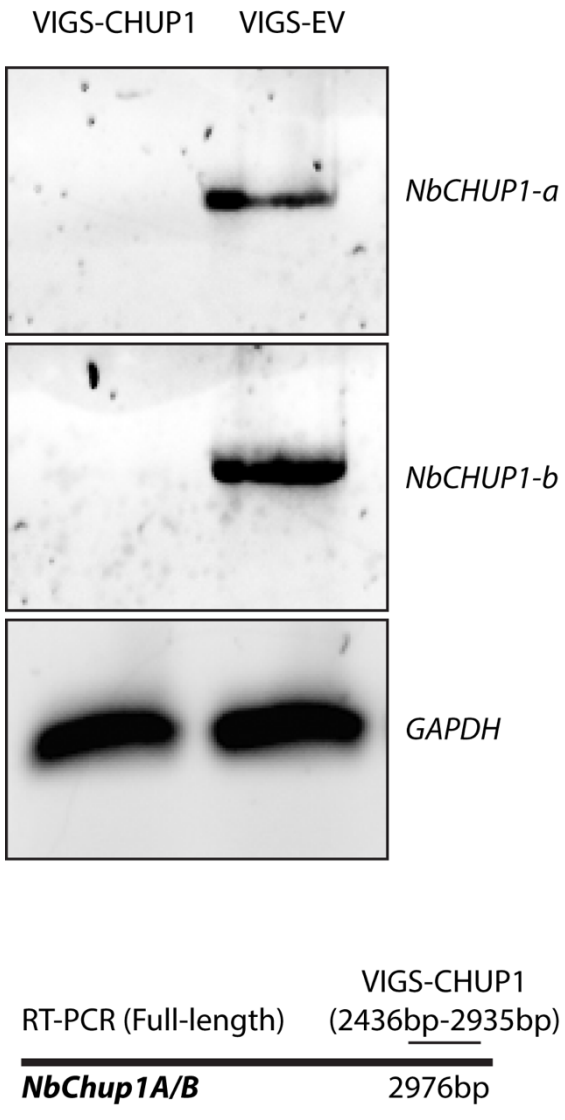

Fig. S6: VIGS-*CHUP1* silences *CHUP1* compared to the EV control. 12 day old transplastomic CpGFP *N. benthamiana* plants, were infiltrated with *Agrobacterium* expressing TRV2:CHUP1 or TRV2:EV. Leaf disks were taken from 5-week old, uninfected, silenced tissue and RNA was extracted. Semi-quantitative RT-PCR of *CHUP1* shows that it was silenced in VIGS-*CHUP1* tissue compared to EV. RT-PCR of housekeeping GAPDH was used as an internal control for cDNA loading. For both, primers that did not amplify the silencing target were use

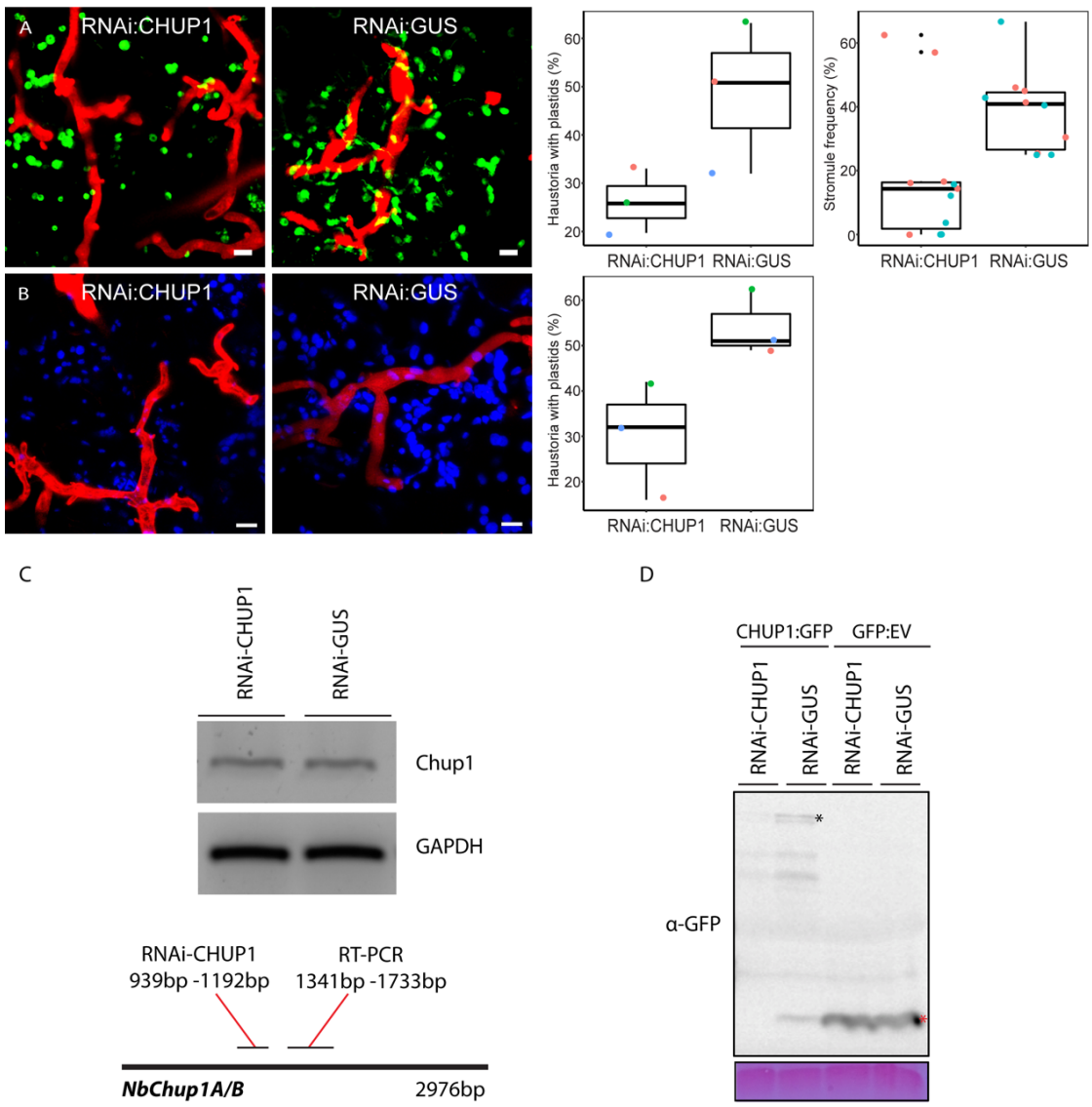

637

638 **Fig. S7: RNAi of CHUP1 suppresses stromule formation and haustorial**
639 **accumulation of chloroplasts** (A) Confocal micrographs of leaf epidermal cells from
640 transplastomic CpGFP *N. benthamiana* plants, in which *CHUP1* is locally silenced
641 (RNAi-CHUP1), 5-7 dpi with *P. infestans* (88069td), with RNAi-GUS included as a
642 control. The first scatter-boxplot depicts the effect of RNAi-CHUP1 silencing on the
643 percentage of haustoria in contact with at least one plastid (27% of n = 237 haustoria),
644 compared to RNAi-GUS control (50% of n = 126 haustoria) ($p < 0.01$). The second
645 scatter boxplot depicts the effect of RNAi-CHUP1 silencing on the percentage of

chloroplasts with one (or more) stromule(s) (18%, *n* = 11 images quantified) compared to RNAi-GUS control (39%, *n* = 10 images quantified) ($p < 0.05$). (B) Confocal micrographs of leaf epidermal cells from WT *N. benthamiana* plants, in which *CHUP1* is locally silenced (RNAi-CHUP1), 5-7 dpi with *P. infestans* (88069td), with RNAi-GUS included as a control. The scatter-boxplot depicts the effect of RNAi-CHUP1 silencing on the percentage of haustoria in contact with at least one plastid (30% of *n* = 392 haustoria), compared to RNAi-GUS control (55% of *n* = 215 haustoria) ($p < 0.01$). Scale bars are 10 µm. (C) Leaf disks were taken from uninfected tissue infiltrated to express the RNAi construct at 6 days post infiltration and RNA was extracted. Following semi-quantitative RT-PCR of *CHUP1* we noted only a slight reduction of *CHUP1* mRNA from RNAi-CHUP1 tissue compared to RNAi-GUS control. However, clear silencing of CHUP1:GFP was seen upon western blotting (D), indicating that the RNAi-CHUP1 hairpin silencing construct mainly acts by blocking CHUP1 translation, as is known to occur for in RNAi(Brodersen et al., 2008).

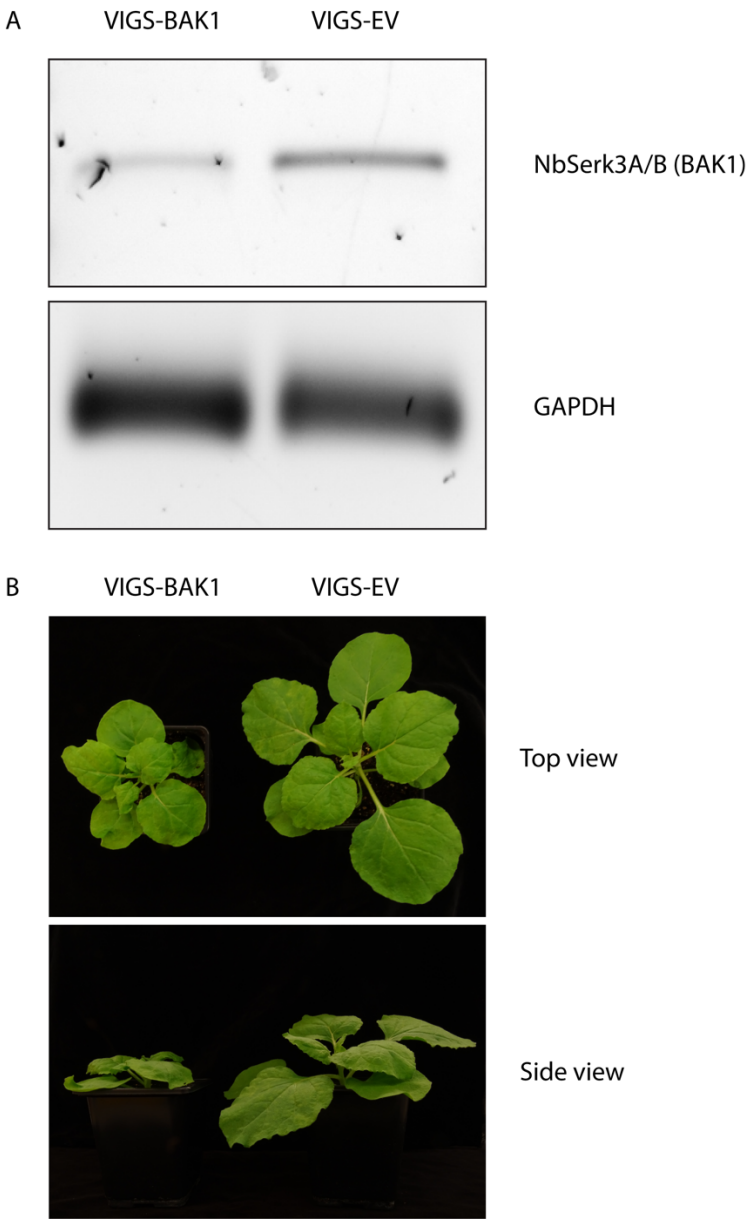

Fig. S8: VIGS-*BAK1* silences *BAK1* compared to the EV control. 12 day old transplastomic CpGFP *N. benthamiana* plants, were infiltrated with *Agrobacterium* expressing TRV2:BAK1 or TRV2:EV. (A) Leaf disks were taken from uninfected, silenced tissue and RNA was extracted. Semi-quantitative RT-PCR of *BAK1* shows that it was silenced in VIGS-*BAK1* tissue compared to EV. RT-PCR of housekeeping GAPDH was used as an internal control for cDNA loading. For both, primers that did not amplify the silencing target were used. (B) Photos of representative *N. benthamiana* plants 5 weeks old, showing symptoms of *BAK1* silencing by VIGS.

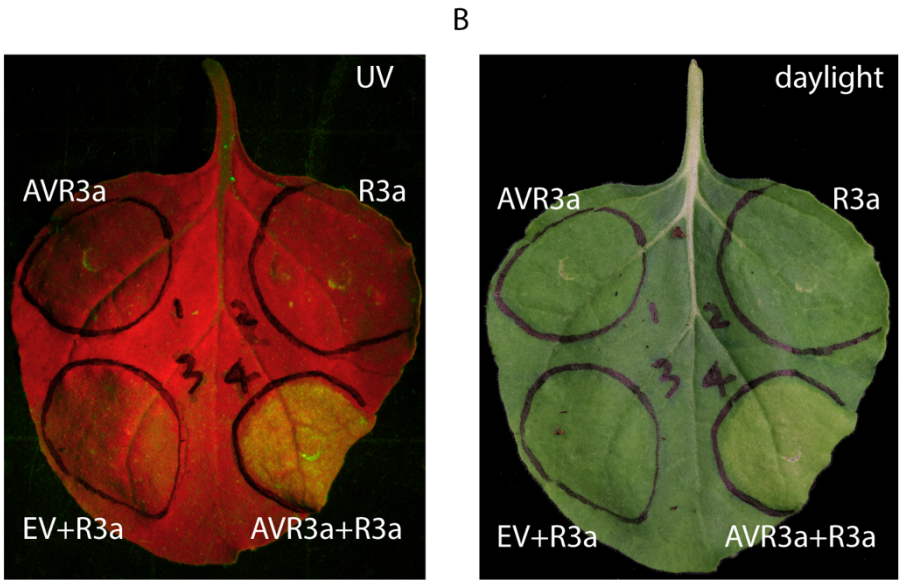

Fig. S9: AVR3a expression triggers HR in an R3a-dependent manner, indicating it is functional. AVR3a or R3a were expressed alone, triggering no HR. EV and R3a also triggered no HR. Only expression of AVR3a with R3a triggered HR, as visible by white light or autofluorescence under UV light.

674 **Table S1. Primers used in this study**

Primer name	Sequence (5´to 3´)
CHUP1-A F	AGGCGGCCGCACTAGTATGATAGTCAGGGTAGGTTTAGTGG
GA_CHUP1_R1	GTTCCAAAACTAGTGATGGCTAC
GA_CHUP1B_F2	GCTCAGAAATGCAGGTGATGGT
GA_CHUP1B_R2	TCCTCGCCCTTGCTCACCATTGATCCTGTTTCTTGTGTATTCTCTTCTCC
VIGS-_CHUP1_F	GGTTGATGAACGAGCTGTCCTCAAG
VIGS_CHUP1_R2	TGACACGACTCCTTAATTCTTCAAAAG
CHP1_RT_F1	ATGATAGTCAGGGTAGGTTTAGTG
BD-CHUP1-REV	ACCAGGTCTCACACCTTGTTCTTGTGTACTCTCT
CHUP1a_RT_F	ATGATCGTCAGGGTAGGTTTAGTGGTTGC
CHUP1a_RT_R	TGTTTCTTGTGTATTCTCTTCTCCTGTTTGT
CHUP1b_RT_F	ATGATAGTCAGGGTAGGTTTAGTGGTTGC
CHUP1b_RT_R	TGTTTCTTGTGTATTCTCTTCTCCTGTTTGT

675

Movie S1: 3D image of Fig. 1A showing chloroplast focal accumulation at haustoria and stromules interacting with each other and other chloroplasts. 3D visualisation comprises Z-stack of confocal images of leaf epidermal cells from transplastomic CpGFP (Yellow) *N. benthamiana* plants infected with red-fluorescent *P. infestans* strain 88069td (Magenta).

Movie S2: 3D time-lapse series showing chloroplasts sieging haustoria. 3D visualisation comprises Z-stack of confocal images of leaf epidermal cells from transplastomic CpGFP (Yellow) *N. benthamiana* plants infected with red-fluorescent *P. infestans* strain 88069td (Magenta).

Movie S3: 3D time-lapse series showing stromules engulfing a haustorium. 3D visualisation comprises Z-stack of confocal images of leaf epidermal cells from transplastomic CpGFP (Yellow) *N. benthamiana* plants infected with red-fluorescent *P. infestans* strain 88069td (Magenta). Grayscale crop of CpGFP signal highlights the extent of chloroplast stromules embracing the haustorium.

Movie S4: 3D image of chloroplast and stromules embracing a haustorium. 3D visualisation comprises Z-stack of confocal images of leaf epidermal cells from transplastomic CpGFP (Yellow) *N. benthamiana* plants expressing PM and EHM marker RFP:REM1.3 (Magenta) infected with WT *P. infestans* 88069.

Movie S5: Time-lapse series of Fig. S1 showing chloroplasts accumulation to a haustorium. Leaf epidermal cells from WT *N. benthamiana* plants expressing PM and EHM marker RFP:REM1.3 (Magenta) and endosomal marker GFP:RAB8 (Yellow) infected with WT *P. infestans* 88069. Blue is chlorophyll autofluorescence, labelling the chloroplasts.

Movie S6: Time-lapse series showing optical trapping of chloroplast in Fig. 1G which escapes the trap and springs back to the haustorium. TIRF microscopy combined with laser capture in leaf epidermal cells from transplastomic CpGFP (channel not shown) *N. benthamiana* plants expressing PM and EHM marker RFP:REM1.3 (Grayscale) infected with WT *P. infestans* 88069. Chloroplast is visible due to chlorophyll autofluorescence overlapping with RFP emission spectrum. Scale bar is 10 µm.

Movie S7: 3D image of Fig. S3 showing chloroplasts form long-distance stromule interactions that can bridge more than one haustorium. 3D visualisation comprises Z-stack of confocal images of leaf epidermal cells from transplastomic CpGFP (Yellow) *N. benthamiana* plants infected with red-fluorescent *P. infestans* strain 88069td (Magenta). 'H' indicates haustorium.

Movie S8: 3D time-lapse series showing dynamic stromule interactions. 3D visualisation comprises Z-stack of confocal images of leaf epidermal cells from transplastomic CpGFP (Yellow) *N. benthamiana* plants infected with red-fluorescent *P. infestans* strain 88069td (Magenta).

Movie S9: Time-lapse series showing optical trapping of chloroplast in Fig. 1H and comigration of a second chloroplast interacting via a stromule-like extension. TIRF microscopy combined with laser capture in leaf epidermal cells from transplastomic CpGFP (Grayscale) *N. benthamiana* plants. Scale bar is 10 µm.

719 **Movie S10: Time-lapse series of Fig. S3 showing collapse of haustorium engulfed**
720 **by a chloroplast.** Leaf epidermal cells from WT *N. benthamiana* plants expressing
721 CHUP1:GFP (Yellow) and PM and EHM marker RFP:REM1.3 (Magenta) infected with
722 WT *P. infestans* 88069. Blue is chlorophyll autofluorescence, labelling the chloroplasts.
723 "H" indicates haustorium that collapses.

724 **Movie S11: Time-lapse series of Fig. S3 showing collapse of haustorium**
725 **associated with a chloroplast.** Leaf epidermal cells from WT *N. benthamiana* plants
726 expressing PM and EHM marker RFP:REM1.3 (Magenta) and endosomal marker
727 GFP:RAB8 (Yellow) infected with WT *P. infestans* 88069. Blue is chlorophyll
728 autofluorescence, labelling the chloroplasts. "H" indicates haustorium that collapses.

729 **Movie S12: Time-lapse series showing synchronised steering of chloroplasts**
730 **away from haustorium.** Leaf epidermal cells from transplastomic CpGFP (Yellow) *N.*
731 *benthamiana* plants expressing PM and EHM marker RFP:REM1.3 (Magenta) and GFP-
732 NbNRC2 (NLR, channel not shown) infected with WT *P. infestans* 88069.

733 **Movie S13: Time-lapse series showing chloroplasts synchronised in pulling away**
734 **from haustorium.** Leaf epidermal cells from transplastomic CpGFP (Yellow) *N.*
735 *benthamiana* plants expressing PM and EHM marker RFP:REM1.3 (Magenta) infected
736 with WT *P. infestans* 88069. "H" indicates haustorium the chloroplasts pull away from in
737 a synchronised manner.